energies

MDPI

Article

New Model of Granite Buried-Hill Reservoir in PL Oilfield, Bohai Sea, China

Daji Jia [1,2,*], Xiaomin Zhu [1,2], Laiming Song [3,4,*], Xu Liang [3,4], Li Li [5,6], Haichen Li [7] and Zhandong Li [8]

1 State Key Laboratory of Petroleum Resources and Prospecting, China University of Petroleum, Beijing 102249, China
2 College of Geosciences, China University of Petroleum, Beijing 102249, China
3 State Key Laboratory of Offshore Oil Exploitation, Beijing 100028, China
4 CNOOC Research Institute Co., Ltd., Beijing 100028, China
5 International Education Exchange Center, Langfang Normal University, Langfang 065000, China
6 Heilongjiang Northeast Petroleum University Science Park Development Co., Ltd., Daqing 163000, China
7 School of Earth and Space Sciences, Peking University, Beijing 100871, China
8 College of Offshore Oil & Gas Engineering, Northeast Petroleum University, Daqing 163318, China
* Correspondence: jiadaji@126.com (D.J.); songlm@cnooc.com.cn (L.S.)

Abstract: The geological estimated hydrocarbon reserves of the Mesozoic granite buried-hill reservoir in the PL oilfield exceed 200 million tons. During the exploration stage, it was commonly considered that the PL buried-hill reservoir should demonstrate a "layered" edge water reservoir mode, because of weathering and tectonics. However, during a later stage, the formation of water was found at structurally high locations, which does not fit the intuition. Therefore, a suitable model is still lacking. Based on the comprehensive information of thin-section, core plug, well logging, and seismic data, etc., the buried-hill of the PL oilfield was re-divided into three northeast–southwest-trending zones. In this model, the reservoir is layered, with each layer having the characteristics of bottom water and two kinds of horizontal and vertical seepage. This new model fits the field-drilling test very well. These insights can effectively guide the exploration and development practice for this kind of buried-hill.

Keywords: granite; buried-hill; oil and gas reservoir; fracture; stratified reservoir model; reservoir model

Citation: Jia, D.; Zhu, X.; Song, L.; Liang, X.; Li, L.; Li, H.; Li, Z. New Model of Granite Buried-Hill Reservoir in PL Oilfield, Bohai Sea, China. *Energies* **2022**, *15*, 5702. https://doi.org/10.3390/en15155702

Academic Editors: Bin Pan, Shaojie Zhang, Hui Gang and Reza Rezaee

Received: 10 June 2022
Accepted: 2 August 2022
Published: 5 August 2022

1. Introduction

Granite oil and gas reservoirs account for about 40% of the bedrock buried-hill reservoirs worldwide, and contribute about 75% of the bedrock oil and gas reserves [1–7]. In recent years, with the discovery of large granite reservoirs in the Bohai Bay Basin and the Pearl River Mouth Basin in China, research about granite reservoirs has increased significantly. The PL buried-hill shown in Figure 1 is one of the important discoveries [8–11]. In this PL oilfield, the geological hydrocarbon reserves of the Mesozoic granite buried-hill reservoir exceed 200 million tons.

During the oil-in-place (OIP) assessment stage, it was considered that the PL granite buried-hill reservoir was layered, but with edge-water characteristics. The model suggested that the granite weathered crust of the oilfield shows a vertical zonation—an extremely strong-weathered zone, a strong-weathered zone, a secondary weathered zone, and a weak-weathered zone, from top to bottom (Figure 1). A stable tight layer exists between the strong-weathered zone and the secondary-weathered zone, which plays the role of longitudinal separation between oil and water. Three reserve units developed in the strong-weathered zone, all of which are proven units. Relatively stable tight zones exist as the separation between the units. The oil bottom or oil–water interface serves as the fluid interface within the unit.

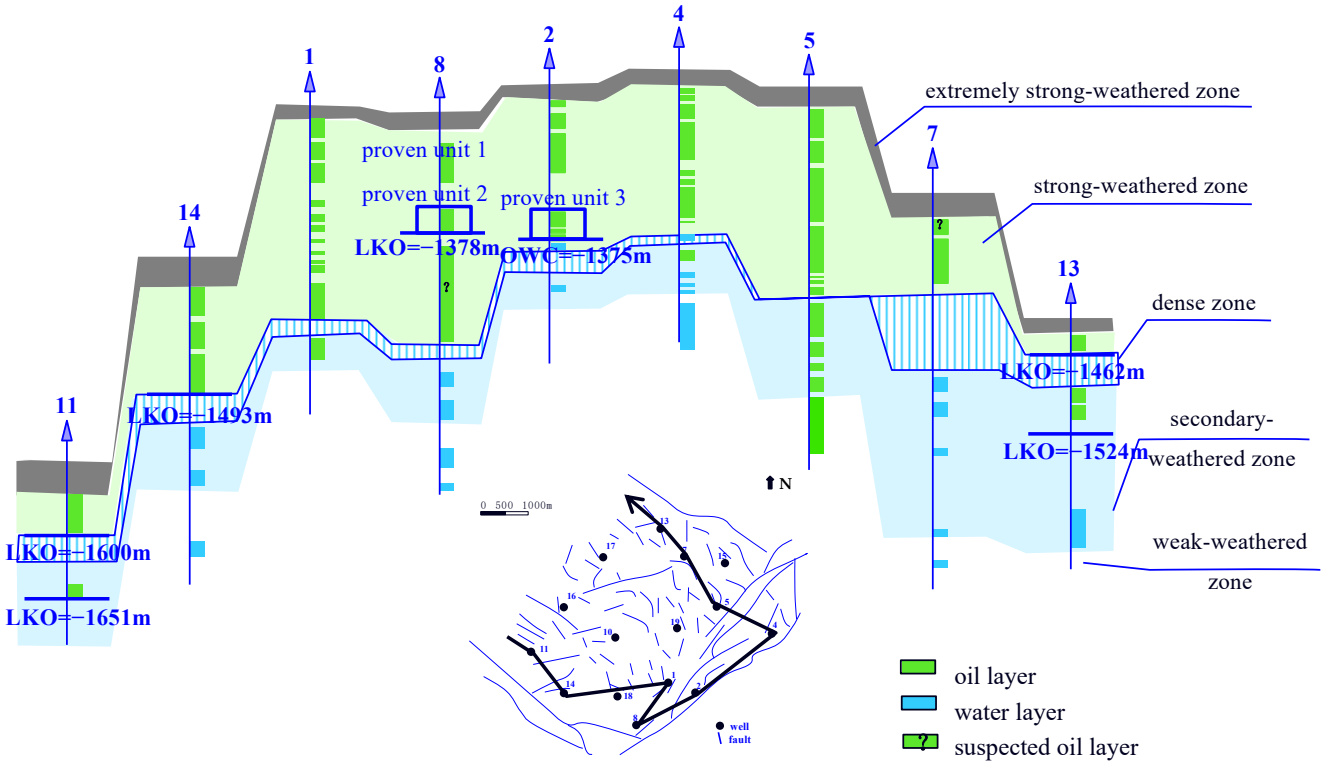

Figure 1. Vertical zoning characteristics of PL oilfield reserves during the oil-in-place assessment stage. LKO refers to the bottom boundary of the oil layer and OWC refers to the oil–water interface.

However, this intuitive mode is in contrast with the following facts. First, water was discovered at the top of this formation, and it is uncertain where the water came from. Secondly, the internal tight layer is relatively heterogeneous, which is different from the so-called one-time intrusion theory [9]. Finally, the drilling data revealed that the fluid distribution in the buried-hill is irregular between different wells. Therefore, the geological characteristics of the PL granite buried-hill reservoir are still unclear. The existing layered mode does not fit this special PL granite buried-hill reservoir.

The primary objective of this work was to establish a new model to describe the PL granite buried-hill reservoir, which would contribute to the strategies of exploration and development in this hydrocarbon formation.

2. Geology

The PL oilfield is located on the Miaoxibei uplift in the Bohai Sea. Its overall structure is a large-scale semi-anticline attached to the large faults at the eastern boundary of the uplift (Figure 2). Its oil source mainly comes from the Shahejie formation in the Bodong sag and Miaoxi sag. As an ancient landform, the buried-hill has been subjected to long-term weathering and erosion. The north–south high point of the buried-hill is a Proterozoic metamorphic rock (Figure 2). The saddle in the middle is a Mesozoic granite intrusion, which is wide and gentle, with an area of more than 140 km^2 (Figure 2). The majority of the saddle is high in the east and low in the west. The drilling revealed that the thickness of the granite body is 139–349 m. The trap area is 90 km^2, the buried depth of the high point is −1220 m (Figure 1), and the closure amplitude is 400 m (Figure 2).

The weathering crust of the buried-hill has mainly developed two sets of fault systems; one is a long-term active NE fault system, and the other is an early active SW and NWW fault system. Long-term active faults control the formation and basic morphology of buried-hills. Early active faults complicate the fault system at the top of the buried-hill, forming a ridge landform and controlling the formation of granite reservoirs.

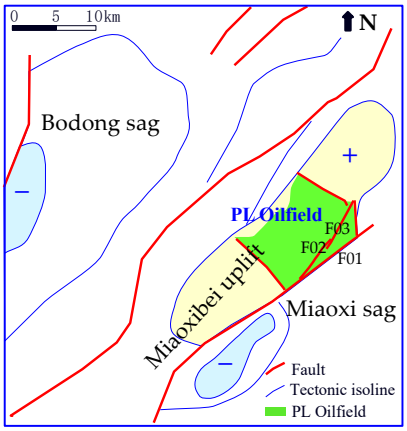

Figure 2. Structural location of PL oilfield.

3. Methodology

By analyzing multi-scale data and integrating dynamic and static multi-dimensional information, a reservoir model of the PL oilfield was studied. The basic data used in this paper include drilling, coring, logging, seismic, and well-testing data. There are 4 cored wells in the PL oilfield, with a footage of 74.87 m, a core length of 53.23 m, and a harvest rate of 71.1%, for which the length of the oil-bearing core was 50.5 m. A total of 270 cores were taken from the rotating shaft wall, with a coring density of 1/5 m–1/10 m, including 129 oil-bearing cores. The cast thin sections were sampled from the core, mainly according to the identification of rock thin sections (SY/T 5368-2000), and the instrument used was a Leica DMRP. In addition to conventional logging data, multipole array acoustic logging, borehole imaging logging, and natural gamma spectroscopy were also used to measure the wells. The three-dimensional seismic data used were collected in 2004, covering an area of 390 km^2. The sampling length was 4000 ms, the sample rate was 2 ms, the trace spacing was 6.25 m, and the shot point spacing was 18.75 m. The pre-stack time migration processing method was adopted. The processed data's recorded length was 3.8 s, the sampling rate was 2 ms, and the processing bin was 25 m × 12.5 m. The test data were relatively rich. Before the test operation, a simple sand control operation was carried out with a sand control pipe being a 16/30 mesh high-quality screen pipe. The dst + pcp testing process was adopted. Pumps of 110 rpm and 140 rpm were used for production.

4. Results and Discussion

4.1. Oil and Water Distribution Characteristics of Buried-Hills

According to the well test results, water formations were found in Wells 2, 7, 14 and 17.

The main characteristics of the 9 wells tested are summarized as follows: (1) The produced fluids were different; Well 5 produced oil, Well 7 produced water, and Wells 2 and 14 produced oil and water. (2) The logging interpretation results at the shot section in Well 2 showed that it was an oil layer. However, water formation was found during the test. (3) The depths of the locations of water formation in each test section were different; the difference between the highest and lowest oil–water interface was over 200 m, and the interface in each well was different (Figure 3).

Based on the logging, testing, and interpretation results from 14 wells, this paper considers that there may be three oil–water interfaces in this area: namely, a high oil–water interface (−1376.6 m), a medium oil–water interface (−1468.4 m), and a low oil–water interface (−1600 m) (Figure 3). The high oil–water interface area, i.e., east area, covers Wells 2 and 4. The middle oil–water interface area, i.e., middle area, covers Wells 1, 5, 7, 10, 14, 15, 18 and 19. The low oil–water interface area, i.e., the west area, covers Wells 11, 16 and 17.

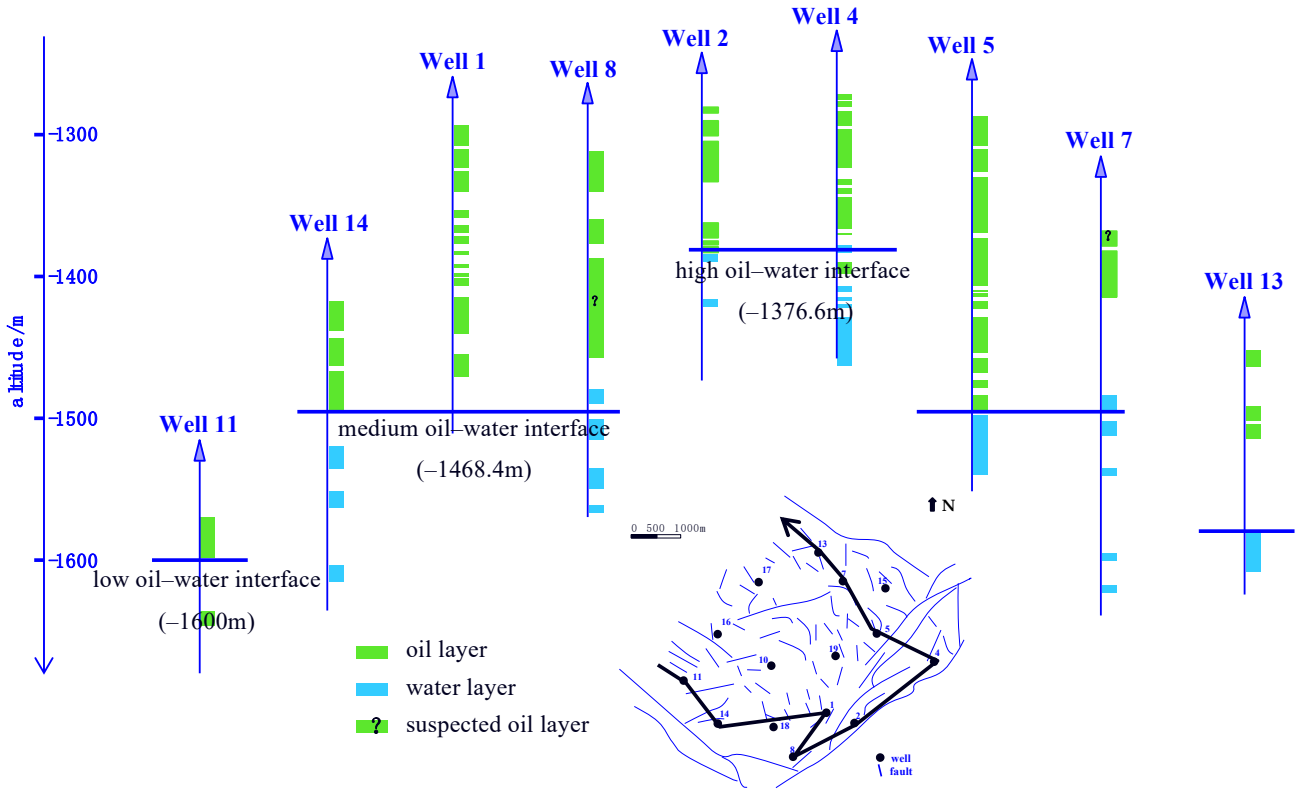

Figure 3. Longitudinal distribution map of oil and water in PL oilfield (OIP oil–water interpretation results). The PL buried−hill reservoir demonstrates a "bulk" bottom water reservoir mode.

As the fluid interface in each well shows different characteristics, the oil–water in this area is vertically distributed. The fluid interface gradually rises from the west to the east. Each zone has a unified oil–water interface (Figure 3). The division of three oil–water distribution zones showed that the granite buried-hill reservoir in the PL oilfield is a bulk reservoir, rather than a stratified reservoir as proposed by previous studies.

The overall characteristics of the 14 wells in this area support the division of the three zones. In addition, the contradiction between the logging and testing interpretation conclusions for individual wells (Figure 3) can be reasonably explained:

(1) Water formation problem in Well 2 during the test on the high oil–water interface (−1376.6 m)

Well 2 was tested twice at the open hole section at 1281–1356 m. The first test lasted for 23 h, and the water formation was 0.85 m^3 (about 5.35 barrels), with a serious sand problems. The second test focused on sand removal. The daily oil production was 31.81 m^3 (about 200.08 barrels), the daily water production was 25.1 m^3 (about 157.87 barrels), and the cl^- concentration was 13,100 mg/L. Through comprehensive analysis, the water from the well was considered formation water. However, the formation water was not from the test section of Well 2, but was caused by the connectivity of high-angle fractures with deep groundwater as a result of the sand removal, with a high flow rate. This conclusion was mainly driven by the following two reasons: ① Well 2 was tested twice at the same section. Water formation was not found in the first test, but was found after the sand removal test. ② The fractures in Well 2 were well-developed. Structural fractures such as vertical fractures and high-angle fractures in the whole PL buried-hill were also well-developed (Figure 4).

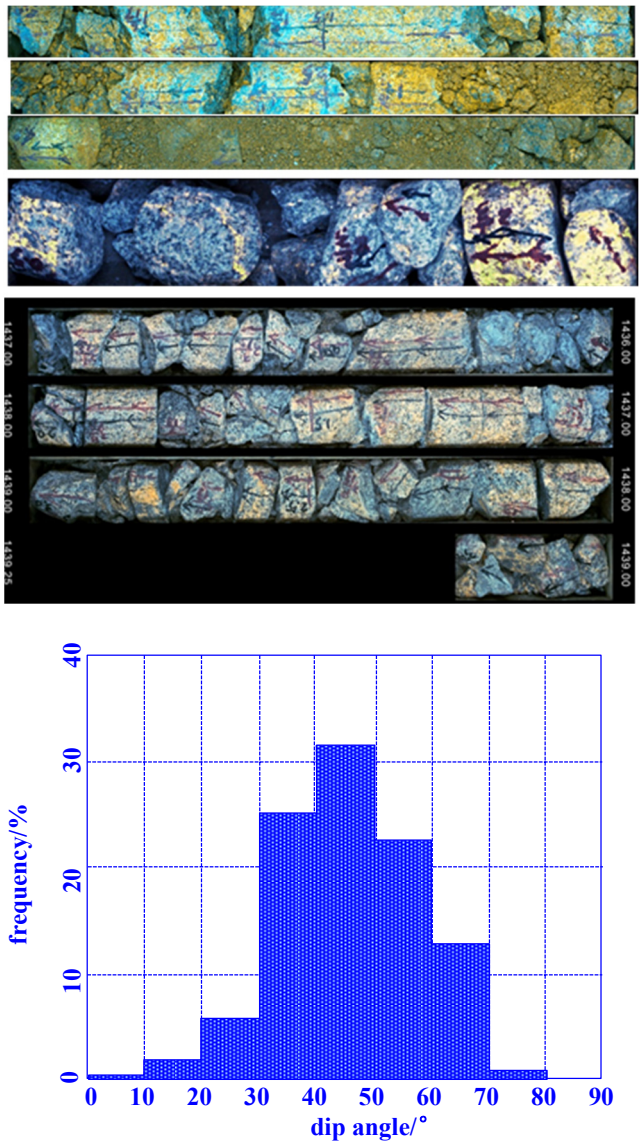

Figure 4. Core photo of the reservoir section and dip angle interpretation of imaging logging. The picture on the left is the core photo of the reservoir section of Well 2. There are 8 boxes of cores in total, and each box is 1 m long. The right figure is the interpretation result of imaging logging, which shows that medium−high angle fractures developed.

(2) The contradiction between the development of oil layers (Wells 5, 10 and 19) below the middle oil–water interface (−1468.4 m) and the development of water layers (Well 14) above the middle oil–water interface.

According to the oil and gas distribution during the logging, and supported by the logging interpretation and test data, it was proven that Wells 1, 5, 7, 10, 14, 15, 18 and 19 have a unified oil–water interface of −1468.4 m. Among these eight wells, five were inconsistent with the existing zoning: ① Oil layers developed under the interface of three wells—Wells 5, 10 and 19 (Figure 3). The analysis results showed that the logging interpretation results of these three wells have multiple solutions. The data support the fact that these oil-bearing sections can be reinterpreted as suspected oil layers. ② A water formation was found in Well 14, whose daily oil production was 2.1 m^3 (about 13.21 barrels) and daily water production was 29.4 m^3 (about 184.92 barrels). A comprehensive analysis showed that the buried-hill faults developed around Well 14, and the characteristics of fault reflection can

be clearly seen on the seismic profile of Well 14 (Figure 5). The water formation during the test was caused by the bottom water in the fault connectivity test section.

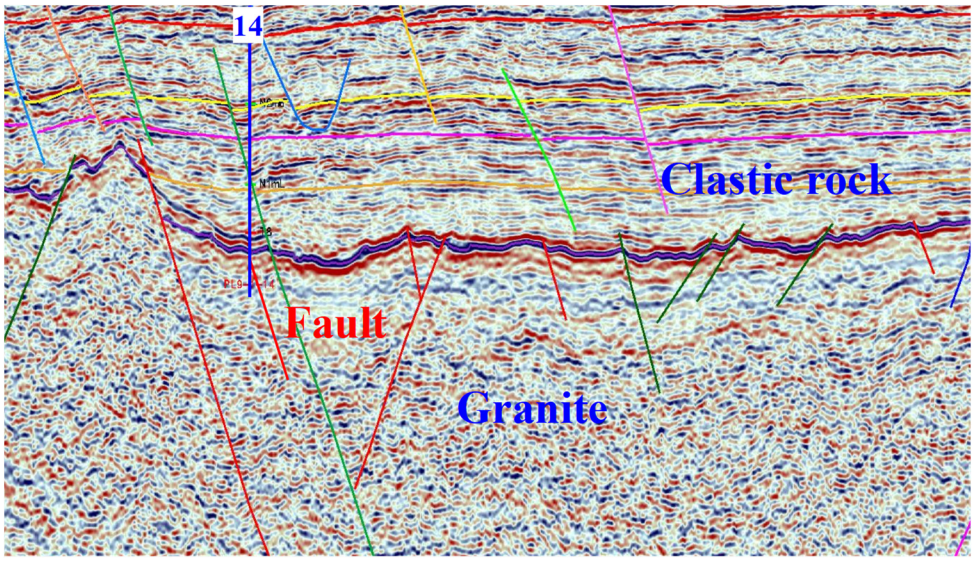

Figure 5. Seismic profile of Well 14 under the seismic sampling rate of 2 ms and the processing bin of 25 m × 12.5 m.

To sum up, the oil–water distribution in the PL buried-hill had the following characteristics: on the plane, it was divided into different zones, and vertically, the oil–water interfaces inside each zone shared the same height (Figure 3) and were bulk reservoirs.

4.2. Controlling Factors of the Distribution of Oil–Water Contacts in Buried-Hill

The analysis showed that the oil–water distribution in the buried-hill is mainly controlled by the granite intrusion mode, faulting, the coupling of fractures with different scales, and the reservoir distribution law. Among these four factors, the first three are the key factors that control the genetic mechanism of the bulk reservoir model. The reservoir distribution law is a representation that restricts the distribution space of oil and water.

4.2.1. The Second-Stage Granite Intrusion Mode Is the Main Factor Responsible for Fluid Zoning and Distribution

The weathered crust of the buried-hill is mainly composed of monzogranite and granodiorite, combined with parts of basic dikes (mainly diabase and lamprophyre). The zircon U–Pb geochronology showed that the age of the granite core in Well 1 was about 165 Ma, which means it was formed in the Middle Jurassic and the intrusion happened in the Yanshanian period. Regional data show that Bohai Bay Basin experienced a series of tectonic events during the Mesozoic and Cenozoic eras, including compression in the overlap between the Late Triassic (T_3) and Yanshanian, a plate force transformation in the early Middle Jurassic (J_{1+2}), extension in the Late Jurassic to Early Cretaceous (J_3–K_1), compression and uplift in the Late Cretaceous (K_2), bidirectional extension in the overlap between the Paleogene and the Himalayan period, unidirectional extension in the Neogene, and overall depression and subsidence in the Quaternary period. Based on the analysis of tectonic history and paleogeomorphic reproduction, this study speculates that the granite intruded in two stages. The composition difference of the intrusive magma in different stages formed the lithologic band of granodiorite in Well 10 and Well 7 (Figure 6).

Through a statistical analysis of the composition of lithologic granite, which covers the majority of the work area, it was found that in the high parts of the ancient landform in the east and the west of the work area, such as in Wells 1, 2, 4, 13, 17, and 19, the lithology is mainly monzogranite, and the content of plagioclase and potassium feldspar in the mineral composition is similar. In the high parts of the ancient landform in the middle of

the work area, i.e., Wells 7 and 10, the lithology is mainly granodiorite (Figures 6 and 7). In terms of mineral composition, the dark minerals in the PL granite buried-hill are relatively well-developed, with an average content of about 5%, among which biotite accounts for the majority with a content of between 1% and 20% and an average content of 4.87%. Hornblende takes the second place, ranging from 1% to 6% and with an average content of 3.88%. Pyroxene is the least abundant, with a content of between 1% and 2% and an average of 1.5%. According to the biotite content of each well within the work area, it was found that the biotite content of most wells is between 3% and 6%, with the only exception being 11% in Well 10. The high content of dark minerals indicates that the buried-hill rocks have strong plasticity and weak brittleness, and fractures have not developed because of the low density of regional structural fractures and the poor connectivity. As the density of Wells 7 and 10 is high (the test proved that the upper part of Wells 7 and 10 are dry layers), it is easy to form a tight rock mass, which can separate the oil from water, leading to the distribution of oil and water on the plane (Figure 8).

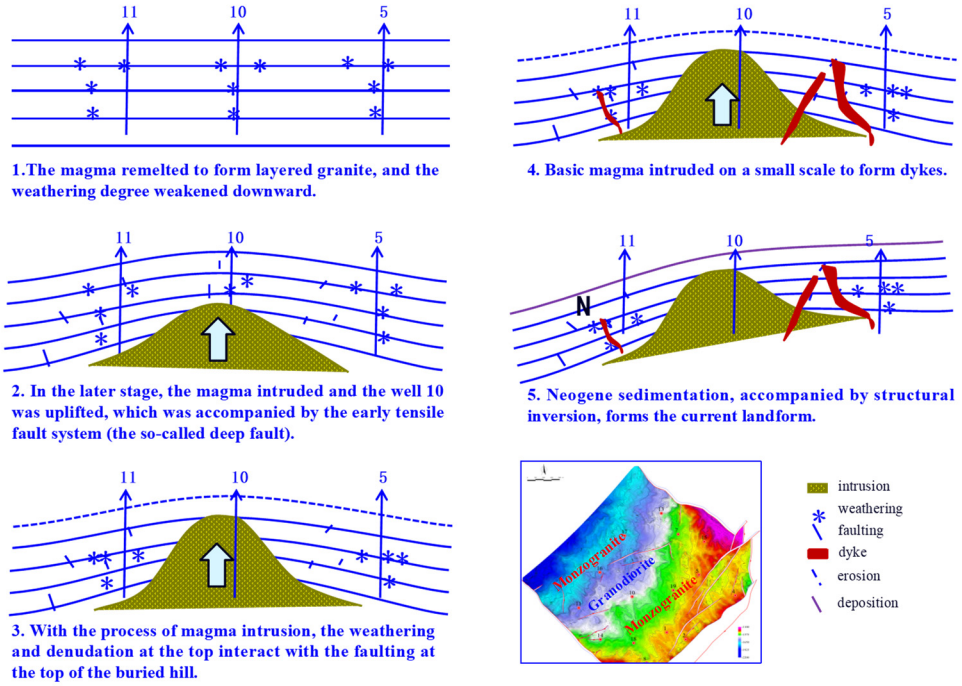

Figure 6. Schematic diagram of formation and evolution mode of the buried-hill in the PL oilfield.

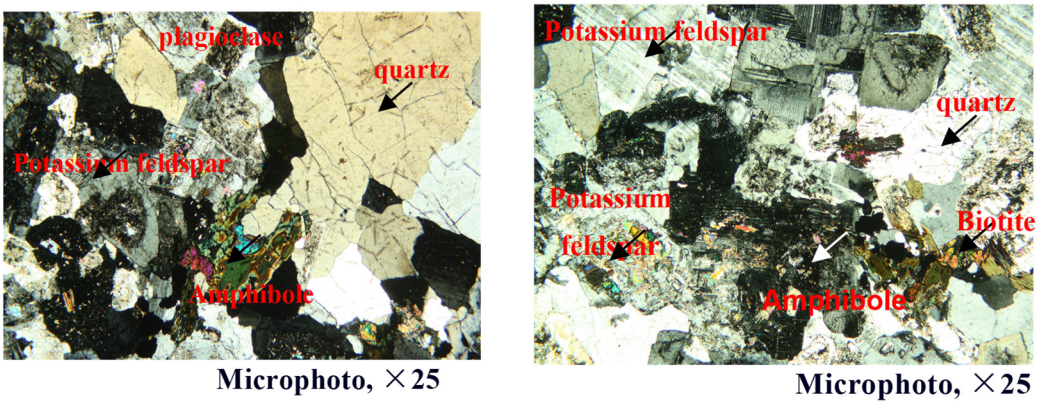

Figure 7. Thin section micrographs of the PL granite buried-hill. The (**left**) figure shows the thin section of Well 13, with a depth of 1502.8 m and a granodiorite lithology; the (**right**) picture shows the thin section of Well 2, with a depth of 1346 m and which is monzogranite.

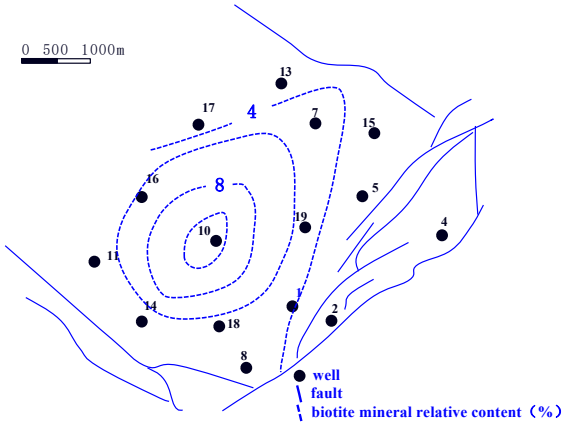

Figure 8. Planar distribution map of relative biotite mineral content in buried-hill.

4.2.2. Lateral Blocking Effect of Long-Term Active Faults

According to tectonic stress field history and the characteristics of the F01 fault, the F02 and F03 faults should belong to the secondary fault of F01—the eastern boundary fault, which was formed during the left-lateral strike-slip movement of the Tanlu fault zone in the Middle Yanshanian [12,13]. In Neogene, the two faults were reactivated under the action of the stress field of the right-lateral strike-slip and eventually connected into one fault, which separated the middle and the east oil–water systems. Due to the long-term weathering and denudation of the granite layer, the two granite walls along the fault surface were gradually transformed by weathering and subsurface erosion. At the same time, with the long-term activity of the two faults, the central cataclastic zone and the fault gouge were gradually formed, and mudstone smearing occurred [14,15]. On the one hand, the physical properties of the two granite walls along the fault improved due to the development of structural fractures, dissolution fractures, and dissolution holes. On the other hand, due to the generation of the cataclastic rock and a fault gouge in the fault center, a blocking surface with poor physical properties was formed.

Field outcrops also proved the possibility of fault-gouge sealing due to long-term active faults. At the Geziwo outcrop [16], the fault bandwidth is about 37 m, in which the 17 m-wide cataclastic zone is composed of fault breccia and a fault gouge and has a lateral blocking effect. The F02 and F03 faults have a much larger fault distance than that of the Geziwo fault, and also demonstrate the characteristics of long-term activity as well as long-term and strong weathering.

4.2.3. The Coupling Effect of Fractures of Different Scales Controls the Internal Connectivity of the Granite Body

The complex fracture system connects the fault block of the buried-hill interiorly, making the reservoir connected horizontally and vertically.

Previous studies have shown that PL buried-hills often develop two fault systems, i.e., a deep fault system and a shallow fault system. The deep fault system is characterized by interlaced development in the near east–west direction and near south–north direction (Figure 9). The shallow fault system is more complex, and mainly develops based on the weathered crust of the buried-hill (Figure 10). The two fault systems were formed in two geological periods. The early active faults were formed in the Middle and Late Yanshanian and the Early Himalayan period, and their extension distance on the plane is short. These faults are mainly in the SN and NWW directions, which complicates the shape of the top surface of the buried-hill. The long-term active faults, mainly in the NE direction, have a long extension distance on the plane and a large space between the individual faults, which controls the sedimentation at the shallow stratum and structural framework. The deep fault system is structurally inherited from the shallow fault system. The overlapping of

multi-stage tectonic movements formed the characteristics of the current fault system in this area; the main fault system is checkerboard-like.

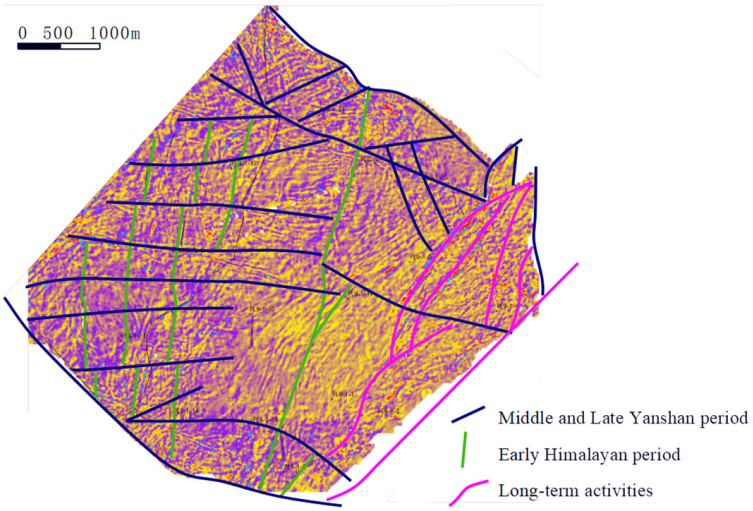

Figure 9. Distribution of deep fault system in PL buried-hill. The fault was interpreted according to 3D root mean square amplitude attribute. It is a time slice map.

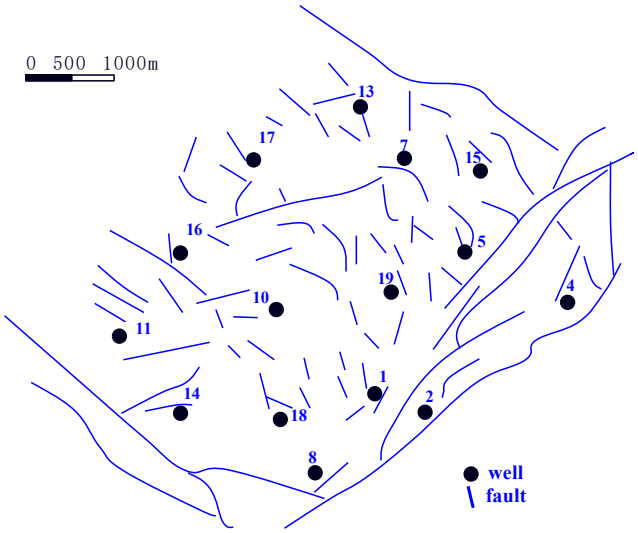

Figure 10. Distribution map of shallow fault system in PL buried-hill (top surface of buried-hill). The fault was interpreted based on 3D post-stack seismic data.

Secondly, faults control the degree of fracture development. The strong-weathered zone is the main development zone of fractures on the weathered crust. According to statistics, the thickness of the strong-weathered zone has an evident relationship with the distance from the well point to the east boundary fault (Figure 11). When the vertical distance from the well point to the east boundary fault increases from hundreds of meters to 7000–8000 m, the thickness of the strong-weathered zone decreases from 160 m to about 10 m.

According to the statistical analysis of the net-to-gross ratio of reservoirs of 15 appraisal wells in the buried-hill section (Figure 12), the effective net gross ratio of the reservoirs in Wells 1, 2, 4, 5, 8, 14, 15, 18 and 19, which are close to the long-term active fault of the buried-hill, is 37–70%, with an average of 55%. The effective net gross ratio of the reservoirs in Wells 7, 10, 11, 13, 16 and 17, which are far from the long-term active fault of the buried-hill, is 7–52%, with an average of 29%. In addition, according to imaging logging,

the direction of reservoir fractures is strongly consistent with the adjacent long-term active faults. Therefore, the distribution of reservoirs on the plane is mainly controlled by the development of long-term active faults.

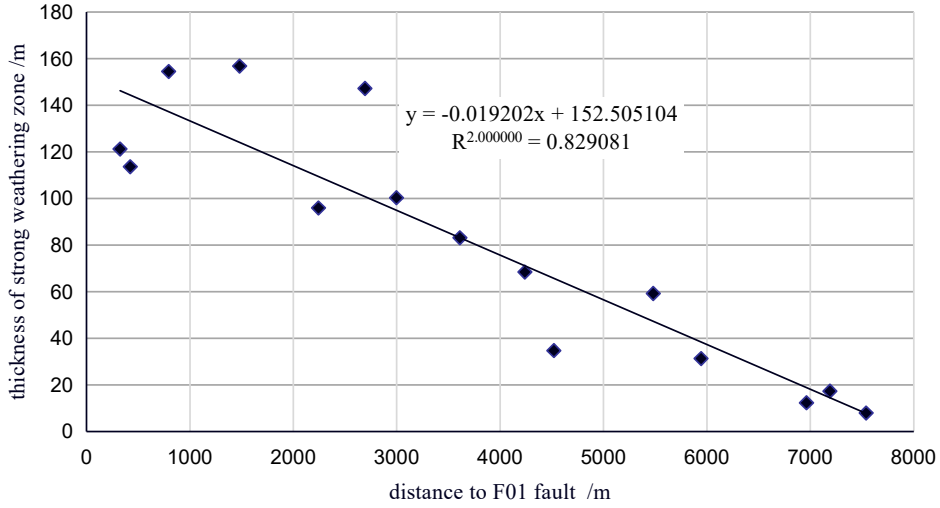

Figure 11. Relationship between thickness of strong-weathered zone and distance to F01 fault (Figure 2). The thickness data of the strong-weathered zone were obtained from integrating core, logging, and seismic data.

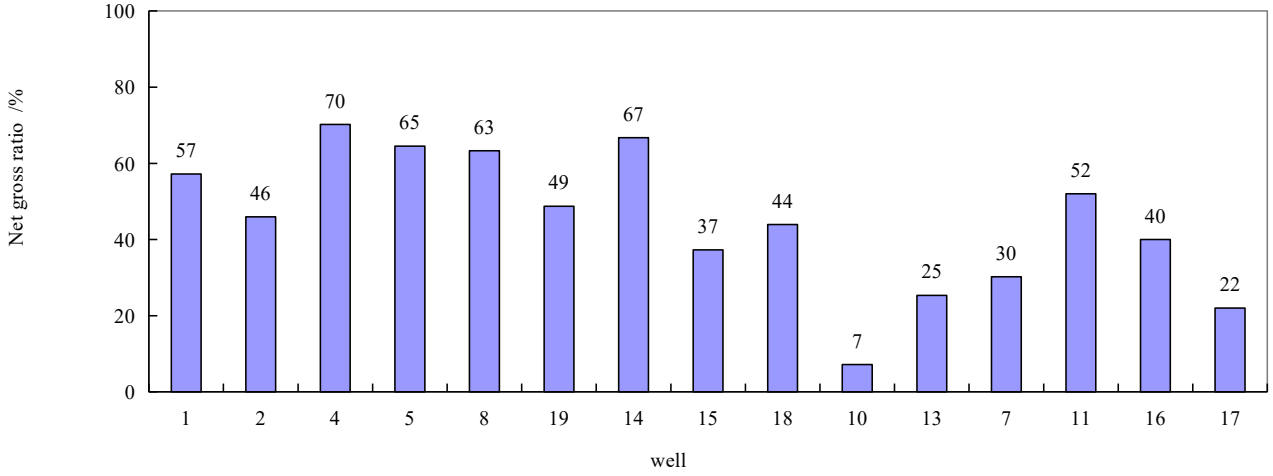

Figure 12. Net gross ratio chart of buried-hill reservoir section in PL oilfield. Net gross ratio data were obtained from logging data.

Thirdly, the cracks in the weathered crust of the buried-hill have an important impact on the reservoir. The Mesozoic reservoir in the PL buried-hill is mainly of the fracture pore type. According to statistics (Figure 13), reservoirs directly related to the fractures account for 85% of the total reservoir. The types of reservoir spaces include fractures, dissolution pores, intergranular pores, and intercrystalline pores (Figure 14), among which (micro) fractures and dissolution pores account for 95% of the whole reservoir space. Further statistics and research show that the major driving force of the dissolution pores is microfractures. According to the statistics of the connectivity of different types of reservoir spaces (isolated type, fracture–hole connected type, and fracture–fracture connected type), the vast majority of reservoir spaces are of a connected type (including the fracture–hole connected type and the fracture–fracture connected type), accounting for 88% of the reservoir spaces in thin sections.

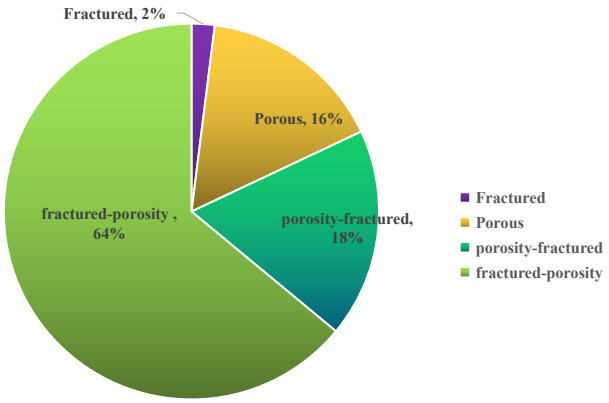

Figure 13. Distribution of PL buried-hill reservoir types. The data were obtained through logging data interpretation.

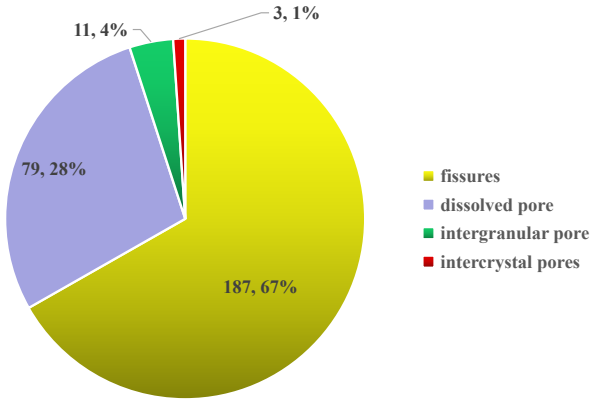

Figure 14. Reservoir pore space types of PL buried-hill. The data were obtained by interpretation of thin sections.

According to above analysis, the internal-connected reservoir pore space of the fault block of the buried-hill was constructed by large faults, small faults, and fracture systems with various scales of fractures.

4.2.4. The Vertical and Plane Distribution of Quasi-Stratified Reservoirs Restricts the Fluid Distribution

Within different zones, the oil and water in buried-hill reservoirs are characterized by bulk distribution. In the fault block, the oil–water distribution is further controlled by the reservoir form. Analysis shows that the weathered crust reservoir in the buried-hill formed by weathering and tectonism has the characteristics of a quasi-stratified distribution.

Comprehensive analysis showed that the PL buried-hill has five layers of geological structures vertically, including alluvial-hillslope sand, an extremely strong-weathered zone, a strong-weathered zone, a secondary-weathered zone, and a weak-weathered zone from top to bottom. Except for the limited distribution of alluvial-hillslope sand, all other zones are horizontally comparable (Figure 1).

The alluvial-hillslope sand is located at the top of the buried-hill, and has been discovered in only four wells so far. Its formation was mainly controlled by the ancient landform and it mostly developed at the foot of the slope and ravine. The sand body encountered in Well 14 during logging was interpreted as an oil layer, so this kind of sand body has development potential.

The extremely strong-weathered zone covers the top of the granite buried-hill in a drape shape. The stratum thickness is 7–14 m, with an average of 10.9 m. According to the drilling characteristics, the thickness of the belt is large at the slope of the ancient landform

and small at the high part. The core proved that the extremely strong-weathered zone has a high shale content and is not capable of forming a reservoir.

The strong-weathered zone is located in the upper part of the granite intrusion. After strong weathering and leaching, the dissolution pores and fractures have become relatively well-developed. The structural fractures developed into a network in which dissolution pores can connect with each other to form a good reservoir pore space, mainly consisting of porous reservoirs and fracture pore reservoirs. The core in this zone is mostly loose sand or fragments. The comprehensive interpretation proved that the reservoir in this zone is developed, with a stable lateral distribution and a good connectivity. The stratum thickness of the strong-weathered zone is 17–157 m, with an average of 100 m. The effective reservoir thickness is 17–133 m, with an average of 76 m. The net gross ratio of the effective reservoir is 35–100%, with an average of 73%. The thickness of a single reservoir is less than 6 m. The interlayer is thin, and the thickness of a proportion of about 53% is less than 2 m.

The weathering and leaching in the secondary-weathered zone are weaker than those in the extremely strong-weathered zone and the strong-weathered zone. In this zone, there are fewer dissolution holes but mainly cracks, the physical properties of which are better. Coring proved that an effective reservoir developed in this zone, but the whole reservoir is relatively tight, mainly consisting of a pore fracture reservoir and a fracture reservoir. A comprehensive analysis showed that the reservoir is poorly developed in this zone, with an unstable horizontal distribution and a poor connectivity. The stratum thickness of the secondary-weathered zone is 30–83 m, while the effective reservoir thickness is 3–55 m. The net gross ratio of the effective reservoir is 6–77%, with an average of 33%.

There are a few drilling wells in the weak-weathered zone. The fractures in this zone are relatively well-developed, with a thicker tight zone and poorer physical properties compared to the other zones. The stratum thickness in this zone is 31–206 m, while the effective reservoir thickness is 0–44 m. The net gross ratio of the effective reservoir is 0–71%, with an average of 30%.

Further statistics revealed that the granite bodies that intruded in the same period have a similar mineral composition. Within the three oil zones formed by the main controlling faults and the granite body (Figure 15), there are intrusions. Within the oil zones, there are no stable layers with consistent characteristics penetrated by wells. For example, within the oil-bearing sections penetrated by the 15 wells in the work area, 0–2 m tight interlayers account for 53%, 2–4 m tight interlayers account for 29%, 4–6 m tight interlayers account for 12%, 6–8 m tight interlayers account for 4.9%, and those thicker than 8 m account for 1.1%. The water formation in Well 2 indicates that the stable interlayer in the strong-weathered zone is almost undeveloped.

4.2.5. Granite Buried-Hill Bulk Reservoir Model

Combined with the oil–water distribution characteristics of the buried-hill and the main controlling factors of oil–water distribution, the plane of the PL buried-hill can be divided into three areas: the east zone, the middle zone, and the west zone. The east and the middle zones are separated by a boundary of long-term active faults, and the middle and west zones are separated by a boundary of a tight lithologic zone, i.e., the granite intrusion in the second stage. The buried-hill has a bulk bottom water reservoir model constrained by a quasi-stratified reservoir (Figure 15). The presumption of the PL buried-hill bulk model solves several key problems: (1) The bulk model can reasonably solve the water formation problem in the two wells (Wells 2 and 14) in the high part of the strong-weathered zone, which means the water formation in the high part of the stratified model will no longer be a problem. This finding lays the foundation for the deployment of a well pattern. (2) The multi-stage granite intrusion model shows that there is no stable transverse tight layer within each weathered zone. The difference in the petrological characteristics between the intrusive rocks of the first and the second stages is important evidence for the zoning of fluids on the plane. The different petrological characteristics (especially the different lithology and dark mineral content) of the two kinds of intrusive rocks result in the different

spatial responses of the PL buried-hill granite to tectonism and weathering. (3) Faulting and modern outcrop investigation showed that, once the long-term active fault is continuously influenced by long-term weathering, it has the tendency to form a fault gouge. This kind of fault is capable of separating the distribution of oil and water in granite. (4) The brittleness of granite determines that all levels of secondary fracture systems in the PL buried-hill are connected with each other, forming a connected body in the three-dimensional space.

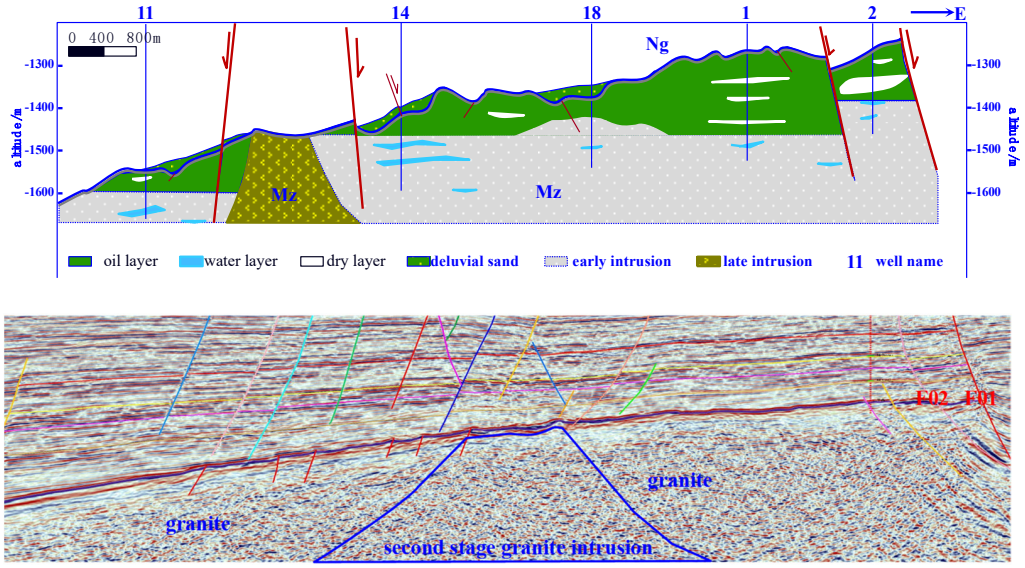

Figure 15. Reservoir model of PL buried-hill. Lithology information was inferred from core, logging, seismic, and geological models, and fluid (oil and water) information was comprehensively analyzed through logging and testing data. On the seismic profile, the reflection characteristics of fault F01 and F02 are relatively clear, but the characteristics of intrusion are fuzzy.

Guided by this model, the north part of the central well zone was selected as the pilot area for the deployment of the well pattern. The relevant scheme has already passed the review. This model promotes the effective development of a buried-hill with technical support.

This study further investigated a main granite and metamorphic granite buried-hill. The results show that all of them have bulk reservoir models, including the Dongshengbao oilfield [2], Qijiagu buried-hill oilfield [17], Shengli Wangzhuang oilfield [2], Caofeidian 1–6 oilfield [18], Chengbei 30 oilfield [19], Xinglongtai buried-hill oilfield [20], Niuxintuo oilfield [3] in Bohai Bay Basin, Baihu oilfield in Vietnam [7], Bongor oilfield in Chad [21], and other granite and metamorphic granite rock buried-hill oilfields [22–31].

5. Conclusions

Based on the systematic investigations of laboratory experiments, field tests, and theoretical analyses for the PL buried-hill hydrocarbon reservoirs, the following views were obtained.

The oil and water in the PL buried-hill has a zoning distribution on the plane. The test and logging interpretation results show that the oil–water interfaces in the west, middle, and east zones of the buried-hill are different. The oil–water distribution in the buried-hill is controlled by a two-stage intrusion mode. The buried-hill has a bottom water reservoir mode. Vertically, there is no obvious interlayer within the quasi-stratified reservoir, and the reservoir is connected into a unified whole by high-angle fractures. The plane is divided into three zones, between which are tight lithologic bodies and long-term active faults serving as the main controlling factors of fluid separation.

These insights will provide significant guidance for the exploration and development of buried-hill hydrocarbon reservoirs around the world.

Author Contributions: Formal analysis, X.Z.; Visualization, X.L., L.L., H.L. and Z.L.; Writing—original draft, D.J.; Writing—review & editing, L.S. All authors have read and agreed to the published version of the manuscript.

Funding: This research was funded by CNOOC. Grant numbers are [2012PFS-017] and [2021KFZL-002].

Conflicts of Interest: The authors declare no conflict of interest.

References

1. Plotnikova, I.N. Nonconventional hydrocarbon targets in the crystalline basement, and the problem of the recent replenishment of hydrocarbon reserves. *J. Geochem. Explor.* **2006**, *89*, 335–338. [CrossRef]
2. Bai, S.; Tang, F. *The Development Models of Buried Hill Fractured Basement Reservoirs*; Petroleum Industry Press: Beijing, China, 1997.
3. Meng, W.; Chen, Z.; Li, P.; Guo, Y.; Gao, X.; Hui, X. Exploration theories and practices of buried-hill reservoirs: A case from Liaohe Depressions. *Pet. Explor. Dev.* **2009**, *36*, 136–143.
4. Yan, F.; Xu, S. Global distribution and hydrocarbon accumulation pattern of basement reservoirs. *Spec. Oil Gas Reserv.* **2011**, *18*, 7–11.
5. Chen, W.; Zhou, W. Important exploration areas in petaliferous basins: The basement hydrocarbon reservoirs. *J. Southwest Pet. Univ.* **2012**, *34*, 17–24. (In Chinese)
6. Pan, J.G.; Hao, F.; Zhang, H.Q.; Wei, S.P.; Zhang, J.L. Formation of granite and volcanic rock reservoirs and their accumulation model. *Nat. Gas Geosci.* **2007**, *18*, 380–385.
7. Deng, Y. Formation mechanism and exploration practice of large-medium buried-hill oil fields in Bohai Sea. *Acta Pet. Sin.* **2015**, *36*, 253–261.
8. Chen, Z.; Mu, Z.; Sun, Y. Characteristics and development strategy of fracture-cavern basement oil reservoir in White Tiger field, Vietnam. *Sino-Glob. Energy* **2009**, *14*, 45–49.
9. Xia, Q.; Zhou, X.; Wang, X.; Liu, P.; Guan, D. Geological characteristics and discovery significance of large-scale and compound oilfield of Penglai 9-1 in Bohai. *Acta Pet. Sin.* **2013**, *34*, 15–23.
10. Xu, G.; Chen, F.; Zhou, X.; Wang, X.; Lan, J.; Wang, G. Hydrocarbon accumulation process of large scale oil and gas field of granite buried hill in Penglai 9-1 structure, Bohai, China. *J. Chengdu Univ. Technol.* **2016**, *43*, 153–162.
11. Hu, Z.; Xu, C.; Bo, Y.; Zhi, H.; Wen, S. Reservoir forming mechanism of Penglai 9-1 granite buried-hills and its oil geology significance in Bohai Sea. *Acta Pet. Sin.* **2017**, *38*, 274–285.
12. Zhou, X.H.; Hu, Z.W.; Wei, A.; Wang, X. Tectonic origin and evolution and their controls on accumulation of Penglai 9-1 large composite oilfield buried hill in Bohai Sea. *Geotecton. Metall.* **2015**, *39*, 680–690.
13. Hou, G.; Qian, X.; Cai, D. The tectonic evolution of Bohai Basin in Mesozoic and Cenozoic time. *Acta Sci. Nat. Univ. Pekin.* **2001**, *37*, 845–851.
14. Wang, Z.; Shang, L.; Gong, L.; Wang, T. Sealing performance evaluation of fault fracture zone of different structures based on geomechanical methods: A case study in M area, Chezhen Sag, Jiyang Depression, Bohai Bay Basin. *Pet. Geol. Exp.* **2019**, *41*, 893–900.
15. Fu, X.; Song, X.; Wang, H.; Liu, H.; Wang, S.; Meng, L. Comprehensive evaluation on hydrocarbon-bearing availability of fault traps in a rift basin: A case study of the Qikou Sag in the Bohai Bay Basin, China. *Pet. Explor. Dev.* **2021**, *48*, 677–686. [CrossRef]
16. Zou, H.; Zhao, C.; Yin, Z. Fracture-occurring outcrop model in Neoarchean crystalline rock-buried hill, Bohai Bay Basin, north China. *Nat. Gas Geosci.* **2013**, *24*, 879–885.
17. Wu, W.; Gao, X. Characteristics and reservoir control effect of interior barriers of Qijia metamorphic buried hill in Liaohe Depression. *Xinjiang Pet. Geol.* **2012**, *33*, 167–169.
18. Chen, H.; Yu, F. Discovery of CFD1-6 granite buried-hill oil pool in western Bohai area. *China Offshore Oil Gas* **1995**, *9*, 111–115.
19. Lu, H. Reservoir Character and Reservoir Forming Pattern of Chengbei 30 Buried Hill. *J. Oil Gas Technol.* **2008**, *30*, 23–27.
20. Zheng, R.; Hu, C.; Dong, X. Analysis of internal structure and reservoir-forming conditions of palaeo-buried hill, Western Liaohe Sag. *Lithol. Reserv.* **2009**, *21*, 10–18.
21. Dou, L.; Wei, X.; Wang, J.; Li, J.; Wang, R.; Zhang, S. Characteristics of granitic basement rock buried-hill reservoir in Bongor Basin, Chad. *Acta Pet. Sin.* **2015**, *36*, 897–904.
22. Tian, S.; Gao, C.; Zha, M. Reservoir-forming characteristics of inner buried hills in Jizhong Depression, Bohai Bay Basin. *Pet. Geol. Exp.* **2012**, *34*, 272–276.
23. Hou, L.; Wang, J.; Zou, C. Controlling factors of weathering volcanic reservoir: An Example from the Carboniferous Kalagang Formation in Santanghu Basin. *Acta Geol. Sin.* **2011**, *85*, 557–568.
24. Zhao, X.; Wu, Z.; Yan, B.; Zhou, C. Distribution and types of buried hill oil-gas reservoir in Jizhong Depression. *Xinjiang Pet. Geol.* **2010**, *31*, 4–6.
25. Deng, Y.; Peng, W. Discovering large buried-hill oil and gas fields of migmatitic granite on Jinzhou 25-1S in Bohai Sea. *China Offshore Oil Gas* **2009**, *21*, 145–150.
26. Su, Y.; Zhu, Z. Percolation characteristics and unstable water injection strategy of fractured buried hill reservoirs: Taking the buried hill reservoir in Bohai JZ25-1S oilfield as an example. *China Offshore Oil Gas* **2019**, *31*, 78–85.

27. Zhou, X.; Xiang, H.; Yu, S.; Wang, G.; Yao, C. Reservoir characteristicsand development controlling factors of JZS Neo-Archean metamorphic buried hill oil pool in Bohai Sea. *Pet. Explor. Dev.* **2005**, *32*, 17–20.
28. Tong, K.; Zhao, C.; Lyu, Z.; Hao, Z.; Sainan, X. Reservoir evaluation and fracture characterization of the metamorphic buried hill reservoir in Bohai Bay. *Pet. Explor. Dev.* **2012**, *39*, 56–63. [CrossRef]
29. Xue, Y.; Li, H. Large condensate gas field in deep Archean metamorphic buried hill in Bohai Sea: Discovery and geological significance. *China Offshore Oil Gas* **2018**, *30*, 1–9.
30. Xu, C.; Du, X.; Liu, X.; Xu, W.; Hao, Y. Formation mechanism of high-quality deep buried-hill reservoir of Archaean metamorphic rocks and its significance in petroleum exploration in Bohai Sea area. *Oil Gas Geol.* **2020**, *41*, 235–247.
31. Song, A.; Yang, J.; Hu, B.; Wang, L.; Lu, X. Zoning characteristics of buried hill reservoir and prediction of favorable reservoir in the western deep water area of South China Sea. *China Offshore Oil Gas* **2020**, *32*, 57–66.